Experimental and Theoretical Study on the OH-Induced Degradation of Piperazine under Simulated Atmospheric Conditions

Wen Tan, Liang Zhu, Tomas Mikoviny, Claus Nielsen, Armin Wisthaler, Barbara D'anna, Simen Antonsen, Yngve Stenstrøm, Naomi Farren, Jacqueline Hamilton, et al.

Experimental and Theoretical Study on the OH-Induced Degradation of Piperazine under Simulated Atmospheric Conditions

Wen Tan,[1§] Liang Zhu,[1§] Claus J. Nielsen,[1] Armin Wisthaler,[1*] Barbara D´Anna,[2] Tomas Mikoviny,[1] Simen Antonsen,[3] Yngve Stenstrøm,[3] Naomi Farren[4] and Jacqueline F. Hamilton[4]*

[1] Section for Environmental Sciences, Department of Chemistry, University of Oslo, P.O.Box. 1033 Blindern, NO-0315 Oslo, Norway.
[2] IRCELYON, CNRS, University of Lyon, F-69626 Villeurbanne, France.
[3] Faculty of Chemistry, Biotechnology and Food Science, Norwegian University of Life Sciences, P.O. Box 5003, N-1432 Ås, Norway.
[4] Wolfson Atmospheric Chemistry Laboratory, University of York, York YO10 5DD, N Yorkshire, United Kingdom.

RECEIVED DATE (10 March 22)

ABSTRACT

The OH-initiated photo-oxidation of piperazine was investigated in chamber experiments at the European Photoreactor (EUPHORE) in Spain and by quantum chemistry methods. The rate coefficient for reaction with OH radicals was determined by the relative rate method to be $k_{\text{OH-piperazine}} = (2.8 \pm 0.6) \times 10^{-10}$ cm^3 molecule^{-1} s^{-1} at 307 ± 2 K and 1014 ± 2 hPa. The reaction was found to proceed via both C-H and N-H abstraction, the latter resulting in the formation of nitroso- and nitro-piperazine. The reaction in the EUPHORE chamber was accompanied by strong particle formation which was induced by an acid-base reaction between photochemically formed nitric acid and the

1 INTRODUCTION

Piperazine (1,4-diazacyclohexane, PZ) is among the amines considered for use in large-scale Carbon capture (CC) to reduce CO_2 emissions from industrial point sources. [1] Tests at the Technology Centre Mongstad (Norway) have established that it is difficult to avoid ppm-level emissions of amines and their process degradation products to the environment during operation of a large-scale capture plant [2] - the concern being the carcinogenic nitrosamines and nitramines either directly emitted or resulting in the subsequent atmospheric photo-oxidation of the emitted amines. [3] The major removal processes of PZ in the atmosphere are uptake in aqueous particles and gas phase reaction with OH radicals during day-time and NO_3 radicals during night-time. The OH rate coefficient for reaction with PZ was recently reported to be ~2.4 × 10^{-10} cm^3 $molecules^{-1}$ s^{-1} at 298 K and to favor C−H abstraction: $k_{N-H}/(k_{N-H} + k_{C-H}) = 0.09 \pm 0.06$. [4]

The PZ nitrosamine (PZ-NO) and nitramine (PZ-NO_2) are both carcinogenic; [3] they result in the following sequence of atmospheric gas phase reactions: [5]

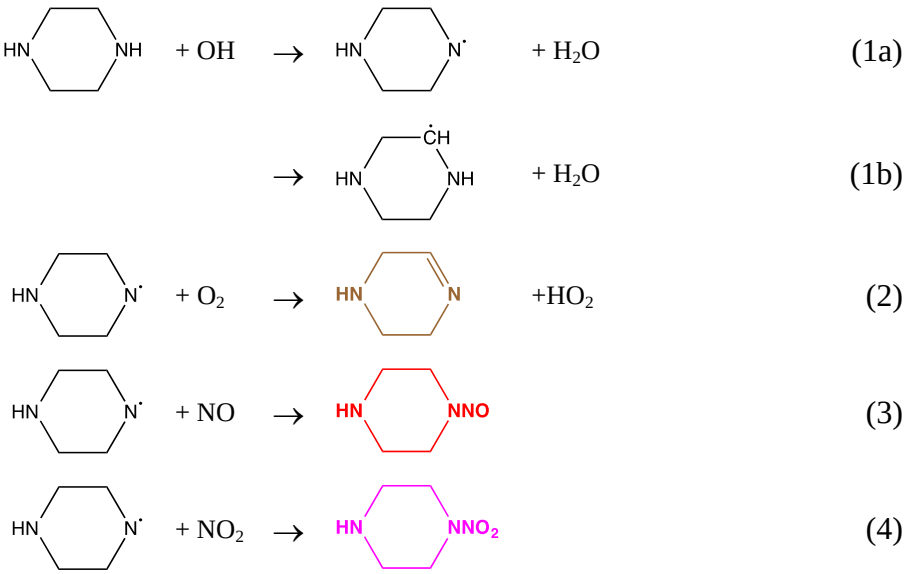

Although the O_2 reaction with N-centered amino radicals, $R_1R_2\dot{N}$, is reported to be around 6 orders of magnitude slower than the corresponding NO and NO_2 reactions, [6] it is still dominating at most atmospheric conditions, and 1-nitrosopiperazine (PZ-NO) and 1-nitropiperazine (PZ-NO_2) will only be minor products in the natural atmospheric photo-oxidation of PZ. Both compounds were observed, but not quantified, in previous piperazine photo-oxidation experiments in the ~200 m^3 EUPHORE atmospheric chamber, [7] and in the more recent experiments employing the ~18 m^3 CSIRO indoor smog chamber. [8]

The open literature includes two theoretical studies on the kinetics of the hydrogen abstraction from PZ by OH radicals, in which the branching between the N-H and C-H abstractions 1a and 1b was predicted to be 0.07 [9] and 0.01 [10], respectively, at 298 K. The latter theoretical study also includes an investigation of the atmospheric degradation following the initial H-abstraction.

In the present communication we report results from a new series of PZ and PZ-NO_2 photo-oxidation and PZ-NO photolysis experiments in the EUPHORE chamber as well as a quantum chemistry based evaluation of the primary products formed in the OH initiated photo-oxidation of PZ.

2 MATERIALS AND METHODS

2.1 Experimental Methods and Chemicals

A series of experiments was carried out in chamber B of the EUPHORE facility in Valencia, Spain. The facility and analytical methods have recently been reported in detail; [11] additional information specific to the present work is found in the Supporting Information.

PZ (Sigma-Aldrich, ReagentPlus®, 99%), acetonitrile (Sigma-Aldrich, LiChrosolv®, ≥99.8%), pyrrole (Sigma-Aldrich, 98 %), 1,3,5-trimethylbenzene (Sigma-Aldrich, 98 %), isoprene (Sigma-Aldrich, analytical standard) and limonene (R-(+), Sigma-Aldrich, analytical standard) were used without further purification. 2-propyl nitrite (isopropyl nitrite, IPN) was synthesized from isopropanol, hydrochloric acid and sodium nitrite, and purified by repeated washing with ice water. The 1:1 nitric acid salt of PZ was prepared by adding a small excess of diluted nitric acid (HNO_3) to diluted PZ followed by rotary evaporation to dryness at 80 °C. Synthesis of 1-nitrosopiperazine and 1-nitropiperazine is described in the Supporting Information.

2.2 Computational Methods

Stationary points on the potential energy surfaces for the atmospheric degradation of piperazine were characterized in M06-2X [12] calculations employing the aug-cc-pVTZ [13-14] basis set. Pre and post reaction complexes were located by following the intrinsic reaction coordinate [15-18] from the saddle points. Reaction enthalpies and proton affinities were calculated using the G4 model chemistry. [19] Additional dipole moments and isotropic polarizabilities, serving as input to prediction of ion-molecule reaction rate coefficients, [20] were obtained in B3LYP/aug-cc-pVTZ calculations, see Table S1 in the Supporting Information. All calculations were performed with Gaussian 09. [21]

Master equation calculations were carried out using the program MESMER 3.0 [22] (Master Equation Solver for Multi-Energy-well Reactions) to simulate the reactions at atmospheric conditions. The required input parameters for molecules, intermediate species and products were obtained from the ab initio calculations.

3 RESULTS

3.1 Computational results

The kinetics of the initial step in the PZ + OH reaction is complicated by PZ existing in two conformations close in energy; a detailed theoretical account of the kinetics is outside the scope of the present work and will be presented elsewhere. [23] Details of the quantum chemistry study of the OH radical initiated atmospheric PZ photo-oxidation are collected in the Supporting Information (including illustrations of the pivotal potential energy surfaces, Figures S1 – S5, and the associated Tables S2 – S5 containing energies, Cartesian coordinates and vibration-rotation data). The quantum chemistry prediction of the major routes in the atmospheric degradation of piperazine are summarized in Scheme 1. The degradation routes largely concord with those established in previous dimethylamine [6, 24-25] and diethylamine [7, 24] photo-oxidation experiments. A recent theoretical study on the OH initiated degradation of piperazine employing the G4 chemistry model did not include the atmospheric fate of the piperazine aminyl radical. [10] The present results also differ with respect to the atmospheric reactions following C-H abstraction from PZ; we find the cyclic alkoxy radical, that ultimately follows C-H abstraction, to be metastable resulting in spontaneous ring opening, and that the major fraction of the resulting $CHONHCH_2CH_2NH\dot{C}H_2$ radical will end up as a diamide. The branching between ring-opening and formation of 1,2,3,6-tetrahydropyrazine (PZ-Im) depends on the NO mixing ratio; master equation calculations employing 5 ppb of NO results in a 15 : 85 branching, whereas a 35 : 65 branching is obtained with 50 ppb of NO.

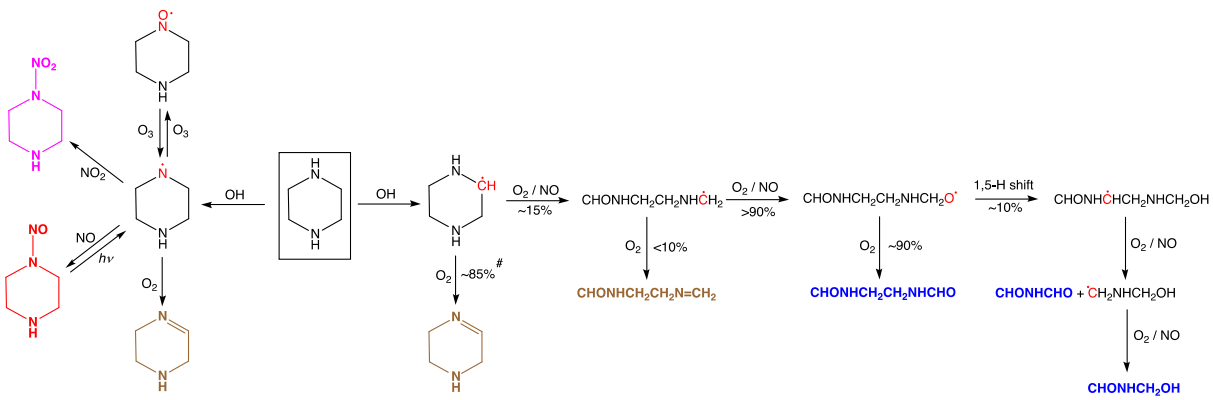

Scheme 1. Quantum chemistry prediction of the major primary products in the atmospheric photo-oxidation of piperazine. [#] The branching between ring-opening and formation of 1,2,3,6-tetrahydropyrazine (PZ-Im) depends on the NO mixing ratio.

The atmospheric fate of PZ-NO_2 was also investigated, and the major photo-oxidation routes for PZ-NO_2, outlined in Scheme 2, parallel those of PZ (Scheme 1) with one exception – the alkyl-radical formed upon ring-opening ejects NO_2 forming an imine. Details of the quantum chemistry study of the OH radical initiated atmospheric PZ-NO_2 photo-oxidation are collected in the Supporting Information.

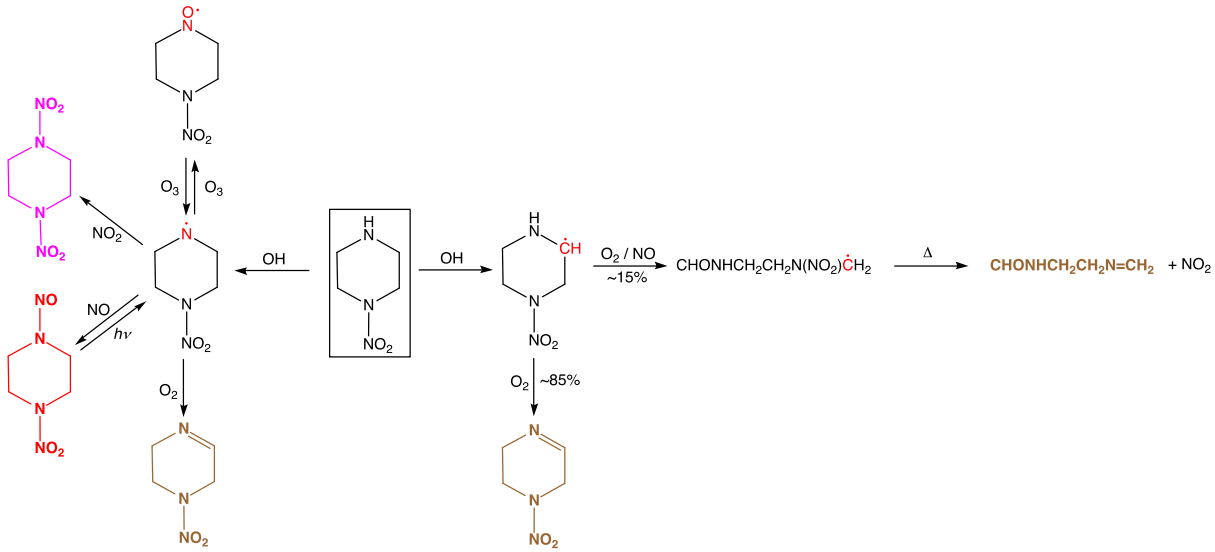

Scheme 2. Quantum chemistry prediction of the major primary products in the atmospheric photo-oxidation of 1-nitropiperazine (PZ-NO_2).

3.2 Experimental results

We first report results from new kinetic studies of the PZ + OH reaction. We then present results from PZ-NO photolysis and from PZ-NO_2 photo-oxidation experiments facilitating interpretation of the PZ photo-oxidation experiments. Finally, we present results from studies of the aerosol formed in the PZ photo-oxidation experiments.

3.2.1 Piperazine + OH reaction kinetics

Two relative rate experiments were carried out in the EUPHORE chamber B in which isoprene, limonene, 1,3,5-trimethylbenzene and pyrrole were used as reference compounds. Acetonitrile was added as inert tracer to monitor the apparent dilution by purified air that is constantly added to compensate for leakage and continuous sampling by the air monitors (k_{OH+CH_3CN} = 2.2 × 10^{-14} cm^3 $molecule^{-1}$ s^{-1} at 298 K). [26] Figure 1 displays the time evolution

of compound-specific PTR-ToF-MS ion signals measured during the second experiment (the first experiment is documented in Figure S6, Supporting Information). The dilution rate due to air replenishment was 8.6 × 10^{-6} s^{-1} in the two experiments; PZ wall loss rates (derived from the reagent decay prior to adding the OH precursor IPN) ranged from 1 to 4 × 10^{-5} s^{-1}. Initial mixing ratios were ~100 ppb for the reference compounds and ~200 ppb for PZ. Average OH densities in the EUPHORE chamber during the periods selected for analyses (9:10 – 9:30 and 14:10 – 14:35 UTC) were around 3 × 10^{6} cm^{-3}; average pressure and temperature in the two experiments were 1014 ± 2 mbar and 307 ± 2 K. The temporal profile of PZ recorded by PTR-ToF-MS matches well the one obtained by a home-built high temperature PTR-MS, indicating an adequate rinstrument esponse time (Figure S7 in the Supporting Information).

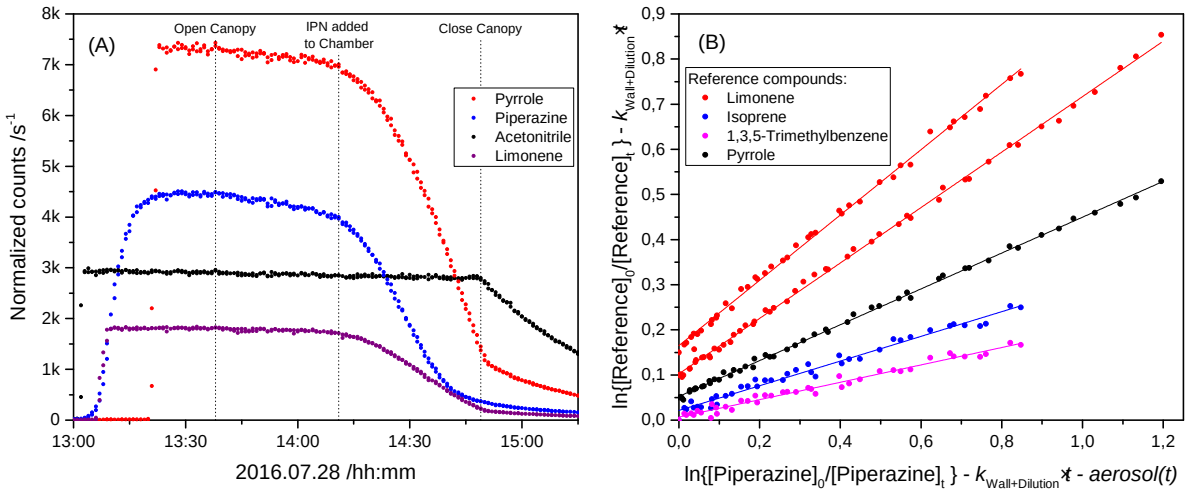

Figure 1. (A): Time evolution of the acetonitrile, pyrrole, piperazine and limonene ion signals at m/z 42.034, 68.050, 87.092 and 137.133, respectively, during the second kinetic experiment on 2016.07.28. (B): Relative rate plot showing the decays of isoprene, limonene, pyrrole and piperazine at 1014 hPa and 307 K in the presence OH radicals. For the sake of clarity the data have been displaced along the abscissa. The data have been corrected for dilution due to chamber air replenishment, for wall loss and for loss to the aerosol, see Supporting Information.

A least–squares fitting of the wall- and dilution loss-corrected data (Figure S8 in the Supporting Information) results in an average $k_{OH+Piperazine}$ = (3.0 ± 0.6) × 10^{-10} cm^3 $molecule^{-1}$ s^{-1} at 307 ± 2 K and 1014 ± 2 hPa. Significant amounts of PZ are, however, transferred from the gas to the particle phase during the periods selected for analysis. Figures S9 and S10 (Supporting Information) show the time evolutions of aerosol mass and the PZ content, and approximately 6.3 and 1.2 % of PZ were actually lost to the aerosol during the two kinetic experiments. Correction for PZ loss to particles during the kinetic experiments was therefore

implemented in the data analysis (Supporting Information) resulting in an average $k_{OH+Piperazine}$ = (2.8 ± 0.6) × 10^{-10} cm^3 $molecule^{-1}$ s^{-1} at 307 ± 2 K and 1014 ± 2 hPa. The present result agrees well with those of Onel et al.,[4] who reported $k(T)$ = (2.37 ± 0.03) × 10^{-10} $(T/298)^{-(1.76\pm0.08)}$ and k = (2.25 ± 0.28) × 10^{-10} cm^3 $molecule^{-1}$ s^{-1} at 307 K from flash photolysis/resonance fluorescence experiments.

3.2.2 1-Nitropiperazine photo-oxidation studies

The atmospheric fate of PZ-NO_2 was investigated in two photo-oxidation experiments – one under high NO_2 levels, the other under high NO levels. Figure S17 in the Supporting Information shows time profiles of the relevant PTR-ToF-MS ion signals observed during a photo-oxidation experiment demonstrating that protonated PZ-NO_2 fragments severely at the instrumental settings employed: 15% *m/z* 132.076 (protonated molecule), 38% *m/z* 86.085 (NO_2 ejection), 30% *m/z* 85.080 (HNO_2 ejection), 4% *m/z* 57.059 (ring fragment), and 13% *m/z* 44.052 (ring fragment). The observed ion signals related to PZ-NO_2 photo-oxidation are summarized in Table S7 in the Supporting Information.

PZ-NO_2 is a very "sticky" compound that transfers relatively fast to particles and wall surfaces (Figure S17) making quantitative conclusions arduous. In line with the extensive fragmentation of protonated PZ-NO_2, most of the ion signals observed during the photo-oxidation corresponds to fragments. It is, however, clear that 1,2-dinitropiperazine (*m/z* 177.055 ($[PZ\text{-}(NO_2)_2,]H^+$) and fragment ions) is a major product, and that also 1-nitro-4-nitrosopiperazine (*m/z* 161.064 ($[NO_2\text{-}PZ\text{-}NO]H^+$) and fragment ions) is formed in the experiments. Surprisingly, the expected key product, 1-nitro-1,2,3,6-tetrahydropyrazine (NO_2-PZ-Im), is not detected as the protonated ion at *m/z* 130.061. Assuming a similar fragmentation of protonated PZ-Im as observed for protonated PZ-NO_2, fragment ions are expected at *m/z* 84.069 (NO_2 ejection), 83.061 (HNO_2 ejection), 55.042 ($CH_2CH_2NHCH^+$), and 42.034 ($CH_2CH_2N^+$). Of these, the *m/z* 83.061, 55.042 and 42.034 are observed.

3.2.3 1-Nitrosopiperazine photolysis studies

Nitrosamines have a characteristic n → π* transition in the UV-A region and photolyse rapidly in natural sunlight; the quantum yield to photo-dissociation of $(CH_3)_2NNO$ following $S_0 \rightarrow S_1(n\pi^*)$ excitation at 363.5 nm was reported to be 1.03 ± 0.10,[27-28] and theory shows that the excited S_1 state is repulsive leading to swift dissociation following excitation.[29] Previous experiments at EUPHORE show that nitroso–dimethylamine, –diethylamine, –

methylethylamine, –methylpropylamine, –methylbutyamine, –morpholine, –piperazine, –piperidine and –pyrazine all photolyze equally fast with $j_{Nitrosamine}/j_{NO_2} = 0.34 \pm 0.04$. [7, 30]

Three photolysis experiments were carried out in the EUPHORE chamber B under conditions that did not allow quantification of the solar radiation. Cyclohexane was added to the chamber (~2 ppm) to enable an estimate of the amount of OH radicals formed following PZ-NO photolysis; the derived OH radical mixing ratio varied between 1 and 4×10^5 cm^{-3} (for details, see the Supporting Information). Taking $k_{PZ\text{-}NO+OH} \approx k_{PZ+OH}$ as a conservative estimate of the PZ-NO reactivity towards OH places an upper level of 2% PZ-NO removal by OH radicals during the photolysis.

Table 1 summarises the observed PTR-TOF-MS ion signals relevant to the PZ-NO photolysis experiments; a more complete list of ion signals observed in the present experiments is found in Table S6 in the Supporting Information, which also includes data obtained in our previous studies. [7] Figure S15 in the Supporting Information illustrates the raw ion signal time profiles; the ion signals growing in upon photolysis fall in 2 categories: (1) the *m/z* 44.052, 83.061, 85.080, 86.085 and 132.074 having time profiles typical of primary products, and (2) the less intense *m/z* 46.030, 74.024, 81.045 and 97.045 with time profiles more resembling those of secondary products.

Table 1. Selected ion signals observed during 1-nitrosopiperazine photolysis experiments.

m/z	Ion sum formula	Interpretation
44.052	$C_2H_6N^+$	Fragment of $[PZ\text{-}NO]H^+$, $[PZ\text{-}NO_2]H^+$and $[PZ\text{-}Im]H^+$
83.061	$C_4H_7N_2^+$	H_2 elimination from $[PZ\text{-}Im]H^+$
85.080	$C_4H_9N_2^+$	Fragment of $[PZ\text{-}Im]H^+$, $[PZ\text{-}NO]H^+$, $[PZ\text{-}NO_2]H^+$
86.085	$C_4H_{10}N_2^+$	Fragment of $[PZ\text{-}NO]H^+$, $[PZ\text{-}NO_2]H^+$
116.079	$C_4H_{10}N_3O^+$	$[PZ\text{-}NO]H^+$
132.074	$C_4H_{10}N_3O_2^+$	$[PZ\text{-}NO_2]H^+$

$[PZ\text{-}NO]H^+$ fragmentation: *m/z* 116.079 (68% protonated molecule); m/z 86.085 (11% NO ejection); *m/z* 85.080 (17% HNO ejection); *m/z* 44.052 (4% ring scission). $[PZ\text{-}NO_2]H^+$ fragmentation: *m/z* 132.076 (17% protonated molecule); m/z 86.085 (40% NO_2 ejection); *m/z* 85.080 (32% HNO_2 ejection); *m/z* 44.052 (11% ring scission).

Two primary products are expected following nitrosamine photolysis: the imine (PZ-Im, 1,2,3,6-tetrahydropyrazine) and the nitramine $PZ\text{-}NO_2$, Scheme 1. Attempts to synthesise PZ-Im were furtile, and fragmentation of protonated PZ-NO and $PZ\text{-}NO_2$ complicates the unambiguous identification of PZ-Im by PTR-TOF-MS. Inspection of the ion signals observed in the PZ-NO photolysis experiments during the time period before opening the chamber canopy (see Figure S11) reveals the $[PZ\text{-}NO]H^+$ fragmentation; the fragmentation of $[PZ\text{-}NO_2]H^+$ was determined in separate experiments with the same instrument parameters,

see later. In summary, the ion signals at *m/z* 44.052, 85.080 and 86.085 all have an origin in both PZ-NO and PZ-NO_2, Table 1. That is, the expected ion signal of protonated PZ-Im at *m/z* 85.080 ($C_4H_9N_2^+$) is also a major fragment of both protonated PZ-NO and PZ-NO_2.

The PZ-NO and PZ-NO_2 fragmentation corrected ion signals are presented in Figure 2, from which it can be seen that there remains significant ion intensities at *m/z* 44.052 and 85.080, whereas *m/z* 86.085 is fully accounted for by PZ-NO and PZ-NO_2. The *m/z* 44.052 ($C_2H_6N^+$) is obviously also a ring scission fragment of $[PZ\text{-}Im]H^+$ and *m/z* 83.061 ($C_4H_7N_2^+$) is explained by H_2-loss from $[PZ\text{-}Im]H^+$.

Figure 2 also includes the derived volume mixing ratios of PZ-NO, PZ-NO_2 and PZ-Im. The mass balance in the photolysis experiments is only around 60% and the discrepancy is primarily due to "missing" PZ-Im, which in part can be explained by partitioning to surfaces and subsequent hydrolysis and/or condensation reactions. The corresponding CHARON PTR-TOF-MS results (see later) suggests a minor presence of PZ-imines in co-existing aerosols.

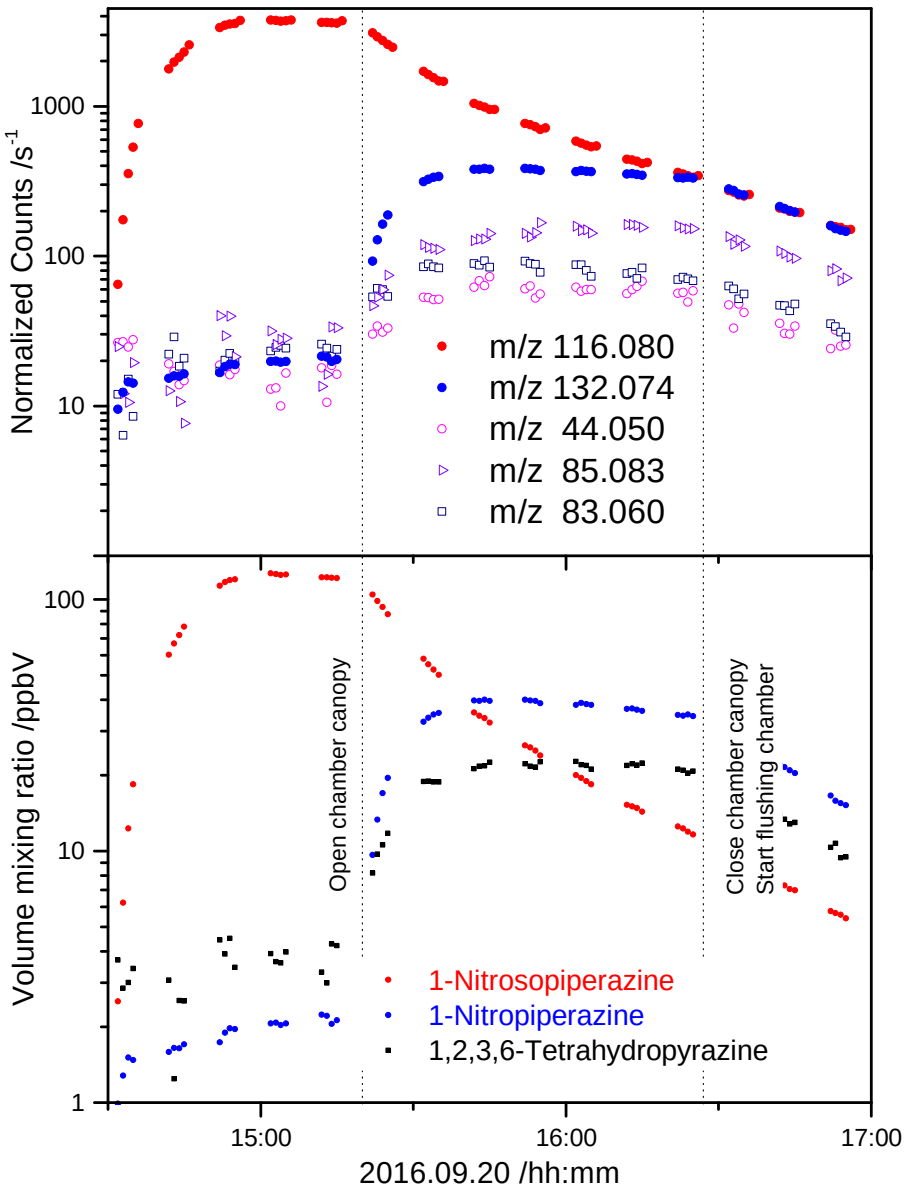

Figure 2. Top: Fragmentation-corrected normalized ion signals during the 1-nitrosopiperazine photolysis experiment on 2016.09.20. Ion signals increasing by less than 2% of the *m/z* 116.080 decrease have been omitted for the sake of clarity. Bottom: Derived volume mixing ratios (ppbV) of 1-nitroso-, 1-nitropiperazine and 1,2,3,6-tetrahydropyrazine during the experiment.

3.2.4 Piperazine photo-oxidation studies

Previous PZ photo-oxidation experiments in the EUPHORE chamber were severely affected by wall adsorption/desorption and particle formation, [7] and a new series of piperazine photo-oxidation experiments was carried out under different, warmer conditions reducing wall adsorption (see Table S8 in the Supporting Information). Piperazine, dissolved in water, was injected into the chamber in a stream of N_2. The detected ion signals can be separated according to their time evolution: (1) signals that appear upon injection of piperazine along with that of protonated piperazine, (2) signals that grow and decrease again

during the photo-oxidation experiment (intermediate products), and (3) signals that grow steadily after opening the chamber canopy. Figure 3 examplifies the observed time evolution of PZ and the major products during a photo-oxidation experiment; the ion signals observed in the new as well as in the previous experiments are collected in Table S9.

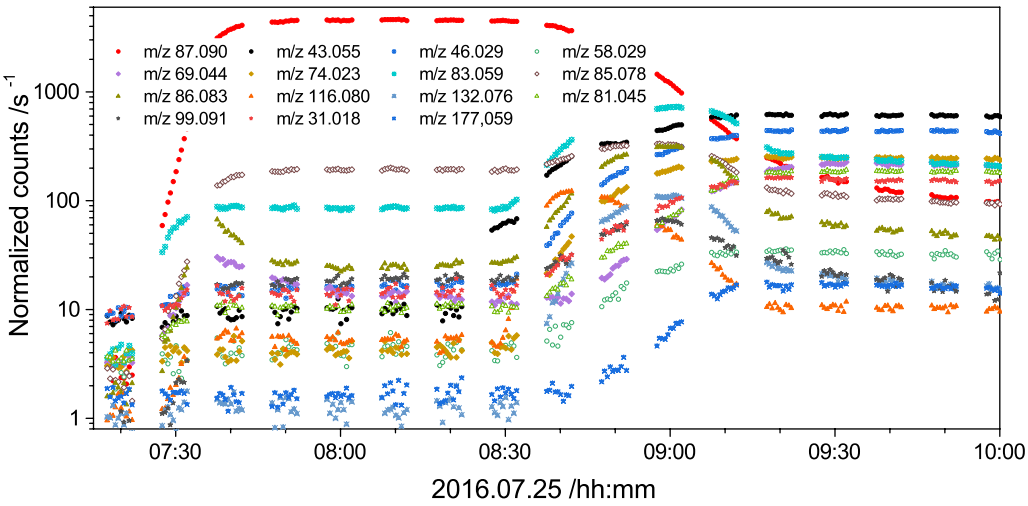

Figure 3. Time evolution of ion signals during the piperazine photo-oxidation experiment on 2016.07.25. Ion signals increasing by less than 2% of the *m/z* 87.090 decrease have been omitted for the sake of clarity.

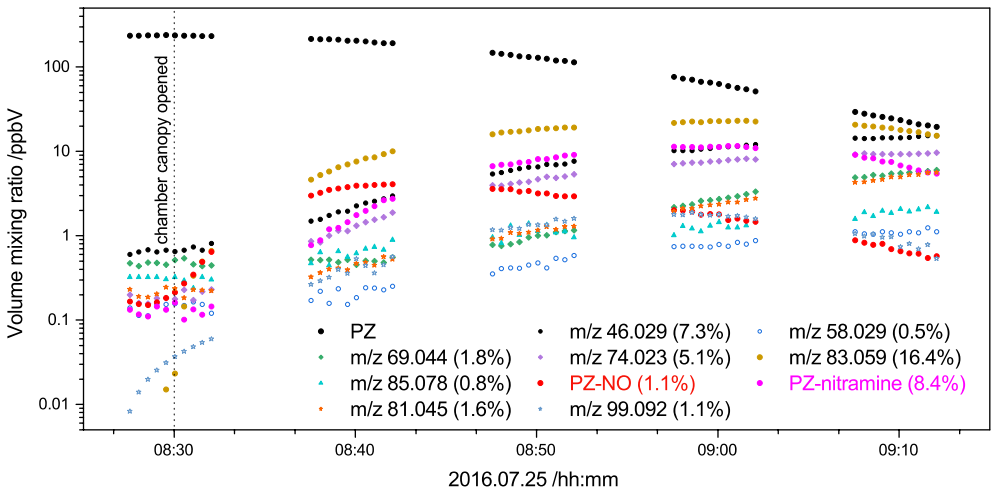

Figure 4. Time evolution of ion signals during the piperazine photo-oxidation experiment on 2016.07.25. Derived volume mixing ratios (ppbV) of piperazine and xxxxx during the experiment. Product yields, calculated after the 30 mins of reaction, are shown in parentheses.

Other major ions in the spectrum include m/z 83.059, *m/z* 74.023 and *m/z* 46.029. We assigned the peak at *m/z* 83.059 to $C_4H_7N_2^+$ whose profile as well as that of *m/z* 81.045 highly correlates with the one of the imine (*m/z* 85.078). This is consistent with the observation in

aforementioned Nitrosopiperazine photolysis section. The peak at *m/z* 74.023 was assigned to *N*-formylformamide (CHONHCHO), a product from the reaction initiated by hydrogen-abstraction from one of the $–CH_2–$ groups in piperazine (Scheme 2). The yield of *m/z* 74.023 was estimated to be 5.1%. The signal at *m/z* 46.029 is identified as formamide (NH_2CHO). Piperazine is expected to condense with formaldehyde, forming $C_5H_{11}N_2^+$ at *m/z* 99.092.

, whereas Table 2 summarises the major PTR-TOF-MS ion signals observed. The $[M\text{-}H_2]^+$ fragment (4.1%) of piperazine upon protonation was taken into consideration

Table 2. Major PTR-TOF-MS ion signals observed during OH initiated piperazine photo-oxidation experiments.

m/z	Ion sum formula	Interpretation
43.0551	$C_3H_7^+$	Fragment of organic species
46.0301	CH_4NO^+	$[NH_2CHO]H^+$
59.0490	$C_3H_7O^+$	$[CHONHCH_2OH]H^+$ - NO_2
69.0447	$C_3H_5N_2^+$	Imidazole ?
74.0243	$C_2H_4NO_2^+$	$[CHONHCHO]H^+$
81.045	$C_4H_5N_2^+$	$[Pyrazine]H^+$
83.0604	$C_4H_7N_2^+$	PZ, H_2 elimination from $[PZ\text{-}Im]H^+$
85.0756	$C_4H_9N_2^+$	From piperazine [a] and PZ-Im, Fragment of $[PZ\text{-}Im]H^+$, $[PZ\text{-}NO]H^+$, $[PZ\text{-}NO_2]H^+$
87.0900	$C_4H_{11}N_2^+$	PZ
99.0561	$C_4H_7N_2O^+$	?
99.0923	$C_5H_{11}N_2^+$	PZ + CH_2O condensation product
115.0862	$C_5H_{11}N_2O^+$	PZ-Im + CH_2O condensation product
116.0787	$C_4H_{10}N_3O^+$	PZ-NO
119.0855	$C_4H_{11}N_2O_2^+$	?
132.0750	$C_4H_{10}N_3O_2^+$	$PZ\text{-}NO_2$

The predicted major products originated from one of the –NH– groups, $PZ\text{-}NO_2$ (m/z 132.077), PZ-NO (m/z 116.084) and the imine, PZ-Im, (m/z 85.078) showed lower presence in spectrum. The former two fragments extensively upon protonation, and the co-existing photolysis caused further signal drop. Upon calibration, the PZ-NO and $PZ\text{-}NO_2$ yield was estimated to be 1.1% and 8.4% in this experiment. It should be note that the numbers present lower limits due to the underestimated wall losses.

The ion pair *m/z* 85.078 and 83.059 partially rationalized the low signal of protonated imine signal at *m/z* 85.078. Taking all factors into consideration, the yield of imine and its derivatives are approximately 17.2%.

One uncertainty factor in data analysis is the peak at *m/z* 43.055 ($C_3H_7^+$), potentially a fragment of higher order of organic species. We decided to leave it out of yield estimation due

to 1), lab calibrations and literature suggest major products such as piperazine-imine, PZ-nitramine, *N*-formylformamide and formamide do not produce such a fragment; 2), the profile of $C_3H_7^+$ peak shows a high correlation with one of acetone, therefore it is suspected the origin of $C_3H_7^+$ peak to be chamber artefacts.

Other minor products are *m/z* 31.018, *m/z* 58.029 and *m/z* 69.044. We assigned this peak to formaldehyde. The *m/z* 69.044 is tentatively assigned to imidazole. The *m/z* 58.029 ($C_2H_4NO^+$) is believed to origin in $CHONHCH_2OH$ elimininating H_2O upon protonation. A detailed mass spectrum and list of the trace products and its possible interpretation is presented in Figure S18 and Table S8.

The present piperazine experiments are hampered by wall adsorption/desorption and particle formation, and the data are insufficient to allow and unambiguously determine the neutral molecules corresponding to the detected ion signals. However, none of the molecular formulae can be related to alkyl nitramines.

3.2.5 Piperazine + OH particle analysis

The aerosol formed in the PZ+OH photo-oxidation was simultaneously detected by three instruments: (1) a PTR-ToF 8000 instrument coupled with a CHemical Analysis of aeRosol ON-line (CHARON) inlet; [31] (2) a compact time-of-flight Aerosol Mass Spectrometer (C-ToF-AMS); and (3) a Scanning Mobility Particle Sizer (SMPS). A detailed description of experimental and instrumental settings is available elsewhere [11]. A relatively good agreement was achieved amongst the results obtained by these three instruments (Figure S19). The aerosol formation proceeded fast and heavily (>10^5 #/cm^3 during all the experiments), as depicted in Figure S20 The C-ToF-AMS measurements indicated that aminium salt is the main consititute in particle phase. In addition to the PZ-nitrate salt, there exists a large fraction of organic species in the aerosol phase. This is in consistence with C-ToF-AMS observations.

To better understand the aerosol composition, we scrutinized the molecular information by CAHRON-PTR-ToF measurement of the piperazine photo-oxidation experiments. The experiments carried out on 26 July 2016, with the highest aerosol yield, was taken as an example. Figure 4 illustrates the quantified mass spectrum of particle-phase products. The most abundant peaks are at *m/z* 87.092 (piperazine) and *m/z* 45.993 (NO_2^+), suggesting piperazine nitrate salt as the main component in aerosols, which accounts for 52.6% in total aerosol mass loading.

The other major peaks are *m/z* 72.042 ($C_3H_6NO^+$), *m/z* 99.078 ($C_5H_{11}N_2^+$, PZ-formaldehyde condensation product), *m/z* 101.071 ($C_4H_9N_2O^+$), *m/z* 115.082 ($C_5H_{11}N_2O^+$), *m/z* 117.067 ($C_4H_9N_2O_2^+$, $CHONHCH_2CH_2NHCHO$), and m/z 142.092 (tentatively assigned to $PZ{\cdot}(H_2O)_2H_3O^+$). In addition, nitramine were detected in particles, *m/*z 132.076 and *m/*z 177.059, assigned to PZ-NO_2 and di-PZ-NO_2, respectively. It is worth to note that the PZ-NO_2 and di-PZ-NO_2 account for 1.7% and 0.88% in total aerosol mass, after fragmentation corrections.

The PZ portioning in aerosol varied from 0.2% (slow IPN, no NOx) to 6% (quick IPN, 90 ppbv NO_2) in PZ+OH photooxidation experiment (see Table S9). Under the assumption that all organic carbon speices in principle should originate from piperazine, this would further increase the portioning of PZ into aerosols to 15.5%. This is justified due to the expected heterogeneous reactions involving primary amines, imines, aldehydes, ketones and carboxylic acids happening on aerosol surfaces.

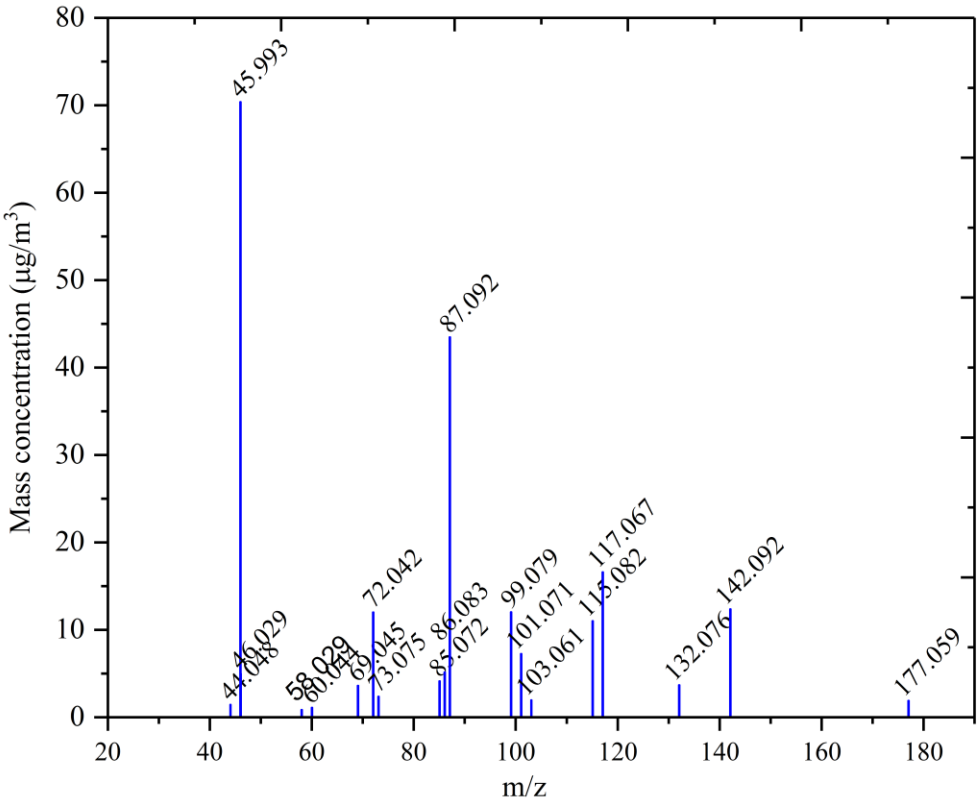

Figure 4. A typical spectrum of particle composition obtained at the highest aerosol loading of piperazine photooxidation under high NOx initial condition, the mass concentration of each *m/z* is calculated by CHARON-PTR-ToF-MS

4. CONCLUSIONS

H-law

5. ATMOSPHERIC IMPLICATIONS

We should mention that there is no experimental value for the corresponding NO_3 rate coefficient, but the empirical correlation between OH and NO_3 rate coefficients for reaction with amines suggests a PZ + NO_3 rate coefficient around 4.6×10^{-11} cm^3 $molecules^{-1}$ s^{-1} at 298 K.[5]

Other

■ Associated content

●, Supporting Information

The Supported Information is available free of charge on the ACS Publications website at DOI: 10.1021/acs/jpca.xxxxxxxx.

■ Author information

Corresponding Author

*E-mail: armin.wisthaler@kjemi.uio.no. Phone: +47-22859139.

*E-mail: claus.nielsen@kjemi.uio.no. Phone: +47 22855680.

ORCID ●,

Armin Wisthaler: 0000-0001-5050-3018

Claus Nielsen: 0000-0002-2962-2634

Notes

The authors declare no competing financial interest

■ Acknowledgments (Word Style "TD_Acknowledgments").

This work is part of the Atmospheric Chemistry of Amines project (ACA) supported by the CLIMIT program under contract 244055 and has received additional support from the Research Council of Norway through its Centres of Excellence scheme, project number 262695.

REFERENCES

1. Wilk, A.; Więcław-Solny, L.; Tatarczuk, A.; Krótki, A.; Spietz, T.; Chwoła, T., Solvent selection for CO2 capture from gases with high carbon dioxide concentration. *Korean Journal of Chemical Engineering* **2017,** *34* (8), 2275-2283.
2. Morken, A. K.; Pedersen, S.; Kleppe, E. R.; Wisthaler, A.; Vernstad, K.; Ullestad, Ø.; Flø, N. E.; Faramarzi, L.; Hamborg, E. S., Degradation and Emission Results of Amine Plant Operations from MEA Testing at the CO2 Technology Centre Mongstad. *Energy Procedia* **2017,** *114* (Supplement C), 1245-1262.
3. Health effects of amines and derivatives associated with CO_2 capture, *Health effects of amines and derivatives associated with CO_2 capture*; The Norwegian Institute of Public Health: 2011.
4. Onel, L.; Dryden, M.; Blitz, M. A.; Seakins, P. W., Atmospheric Oxidation of Piperazine by OH has a Low Potential To Form Carcinogenic Compounds. *Environmental Science & Technology Letters* **2014,** *1* (9), 367-371.
5. Nielsen, C. J.; Herrmann, H.; Weller, C., Atmospheric chemistry and environmental impact of the use of amines in carbon capture and storage (CCS). *Chem. Soc. Rev.* **2012,** *41* (19), 6684-6704.
6. Lindley, C. R. C.; Calvert, J. G.; Shaw, J. H., Rate Studies of the Reactions of the $(CH_3)_2N$ Radical with O_2, NO, and NO_2. *Chem. Phys. Lett.* **1979,** *67* (1), 57-62.
7. Atmospheric Degradation of Amines (ADA), *Atmospheric Degradation of Amines (ADA)*; ISBN 978-82-992954-7-5, http://urn.nb.no/URN:NBN:no-30510; University of Oslo: Oslo, 2012.
8. White, S. J.; Azzi, M.; Angove, D. E.; Jamie, I. M., Modelling the photooxidation of ULP, E5 and E10 in the CSIRO smog chamber. *Atmos. Environ.* **2010,** *44* (40), 5375-5382.
9. Sarma, P. J.; Gour, N. K.; Bhattacharjee, D.; Mishra, B. K.; Deka, R. C., Hydrogen atom abstraction from Piperazine by hydroxyl radical: a theoretical investigation. *Mol. Phys.* **2017,** *115* (8), 962-970.
10. Ren, Z.; da Silva, G., Atmospheric Oxidation of Piperazine Initiated by OH: A Theoretical Kinetics Investigation. *ACS Earth and Space Chemistry* **2019**.
11. Tan, W.; Zhu, L.; Mikoviny, T.; Nielsen, C. J.; Wisthaler, A.; Eichler, P.; Muller, M.; D'Anna, B.; Farren, N. J.; Hamilton, J. F., et al., Theoretical and Experimental Study on the Reaction of tert-Butylamine with OH Radicals in the Atmosphere. *The Journal of Physical Chemistry A* **2018**.
12. Zhao, Y.; Truhlar, D. G., The M06 suite of density functionals for main group thermochemistry, thermochemical kinetics, noncovalent interactions, excited states, and transition elements: two new functionals and systematic testing of four M06-class functionals and 12 other functionals. *Theoretical Chemistry Accounts* **2008,** *120*, 215-241.
13. Dunning, T. H., Jr., Gaussian basis sets for use in correlated molecular calculations. I. The atoms boron through neon and hydrogen. *J. Chem. Phys.* **1989,** *90* (2), 1007-23.
14. Kendall, R. A.; Dunning, T. H., Jr.; Harrison, R. J., Electron affinities of the first-row atoms revisited. Systematic basis sets and wave functions. *J. Chem. Phys.* **1992,** *96* (9), 6796-806.
15. Fukui, K., The path of chemical reactions - the IRC approach. *Accounts of Chemical Research* **1981,** *14* (12), 363-368.
16. Hratchian, H. P.; Schlegel, H. B., Accurate reaction paths using a Hessian based predictor–corrector integrator. *The Journal of Chemical Physics* **2004,** *120* (21), 9918-9924.

17. Hratchian, H. P.; Schlegel, H. B., *Theory and Applications of Computational Chemistry: The First 40 Years*. Elsevier: Amsterdam, 2005.
18. Hratchian, H. P.; Schlegel, H. B., Using Hessian Updating To Increase the Efficiency of a Hessian Based Predictor-Corrector Reaction Path Following Method. *Journal of Chemical Theory and Computation* **2005,** *1* (1), 61-69.
19. Curtiss, L. A.; Redfern, P. C.; Raghavachari, K., Gaussian-4 theory. *Journal of Chemical Physics* **2007,** *126*, 084108.
20. Su, T., Parametrization of kinetic energy dependences of ion–polar molecule collision rate constants by trajectory calculations. *The Journal of Chemical Physics* **1994,** *100* (6), 4703-4703.
21. Frisch, M. J.; Trucks, G. W.; Schlegel, H. B.; Scuseria, G. E.; Robb, M. A.; Cheeseman, J. R.; Scalmani, G.; Barone, V.; Mennucci, B.; Petersson, G. A., et al. *Gaussian 09, Revision B.01*, Gaussian, Inc., Wallingford CT: 2009.
22. Glowacki, D. R.; Liang, C.-H.; Morley, C.; Pilling, M. J.; Robertson, S. H., MESMER: An Open-Source Master Equation Solver for Multi-Energy Well Reactions. *The Journal of Physical Chemistry A* **2012,** *116* (38), 9545-9560.
23. Bunkan, A. J. C.; Nielsen, C. J., *to be published*.
24. Pitts, J. N.; Grosjean, D.; Vancauwenberghe, K.; Schmid, J. P.; Fitz, D. R., Photooxidation of Aliphatic Amines under Simulated Atmospheric Conditions - Formation of Nitrosamines, Nitramines, Amides, and Photochemical Oxidant. *Environmental Science & Technology* **1978,** *12* (8), 946-953.
25. Summary Report: Photo-oxidation of Methylamine, Dimethylamine and Trimetahylamine. Climit project no. 201604, *Summary Report: Photo-oxidation of Methylamine, Dimethylamine and Trimetahylamine. Climit project no. 201604*; NILU OR 2/2011, ISBN 978-82-425-2357-0; NILU: 2011.
26. Atkinson, R.; Baulch, D. L.; Cox, R. A.; Crowley, J. N.; Hampson, R. F.; Hynes, R. G.; Jenkin, M. E.; Rossi, M. J.; Troe, J., Evaluated kinetic and photochemical data for atmospheric chemistry: Volume II - gas phase reactions of organic species. *Atmospheric Chemistry and Physics* **2006,** *6*, 3625-4055.
27. Geiger, G.; Stafast, H.; Bruehlmann, U.; Huber, J. R., Photodissociation of dimethylnitrosamine. *Chem. Phys. Lett.* **1981,** *79* (3), 521-524.
28. Geiger, G.; Huber, J. R., Photolysis of Dimethylnitrosamine in the Gas-Phase. *Helv. Chim. Acta* **1981,** *64* (4), 989-995.
29. Pelaez, D.; Arenas, J. F.; Otero, J. C.; Soto, J., A complete active space self-consistent field study of the photochemistry of nitrosamine. *J. Chem. Phys.* **2006,** *125* (16).
30. Atmospheric Chemistry – Nitrosamine Photolysis. Final report, *Atmospheric Chemistry – Nitrosamine Photolysis. Final report*; Tel-Tek report no. 2211030-NP07 v2; Tel-Tek 2011.
31. Eichler, P.; Müller, M.; D'anna, B.; Wisthaler, A. J. A. M. T., A novel inlet system for online chemical analysis of semi-volatile submicron particulate matter. **2015,** *8* (3), 1353-1360.